

Role of the electric field in surface electron dynamics above the vacuum level

J. I. Pascual,¹ C. Corriol,² G. Ceballos,³ I. Aldazabal,⁴ H.-P. Rust,⁵ K. Horn,⁵ J. M. Pitarke,^{6,7} P. M. Echenique,^{4,7} and A. Arnau^{4,7}

¹*Institut für Experimentalphysik, Freie Universität, Arnimalle 14, D-14195 Berlin, Germany*

²*Donostia International Physics Center (DIPC), San Sebastian, Spain*

³*Istituto Nazionale per la Fisica della Materia TASC, Area Science Park, I-34012 Trieste, Italy*

⁴*Departamento de Física de Materiales, UPV/EHU, San Sebastian E-20080, Spain*

⁵*Fritz-Haber-Institut der Max-Planck-Gesellschaft, Faradayweg 4-6, D-14195 Berlin, Germany*

⁶*Materia Kondensatuaren Fisika Saila, UPV/EHU, Bilbao, Spain*

⁷*Unidad de Física de Materiales, Centro Mixto CSIC-UPV/EHU, San Sebastián, Spain*

(Received 27 November 2006; revised manuscript received 7 February 2007; published 30 April 2007)

Scanning tunneling spectroscopy is used to study the dynamics of hot electrons trapped on a Cu(100) surface in field-emission resonances (FERs) above the vacuum level. Differential conductance maps show isotropic electron interference wave patterns around defects whenever their energy lies within a surface-projected band gap. Their Fourier analysis reveals a broad wave-vector distribution, interpreted as due to the lateral acceleration of hot electrons in the inhomogeneous tip-induced potential. A line-shape analysis of the characteristic constant-current conductance spectra permits establishing the relation between apparent width of peaks and intrinsic linewidth of FERs, as well as the identification of the different broadening mechanisms.

DOI: [10.1103/PhysRevB.75.165326](https://doi.org/10.1103/PhysRevB.75.165326)

PACS number(s): 73.20.At, 68.37.Ef, 71.20.Be

I. INTRODUCTION

A detailed knowledge of the electron dynamics at surfaces is crucial for an understanding of a large variety of processes, ranging from electron scattering at surfaces to charge transport dynamics across interfaces, relevant to design electronic devices.^{1,2} Electrons trapped in unoccupied long-lived resonances represent an interesting workbench. They favor the localization of photoinjected electrons at molecular resonances, thus enhancing the catalytic activity of metals.³ They also represent a valuable probe to investigate the rich phenomenology behind charge injection and hot-electron quenching. Experimental techniques such as inverse photoemission,⁴ two-photon photoemission,⁵ or ballistic electron scattering⁶ have been traditionally used to study hot-electron dynamics at surfaces.

Recently, scanning tunneling spectroscopy (STS) has proved to be a useful tool to provide quantitative information about the electronic structure⁷⁻¹² and also the electron and hole dynamics at metal surfaces.¹³⁻¹⁷ In most cases, these studies have been restricted to low applied bias voltages, where the applied electric field does not play an important role.¹⁸ A renewed interest has emerged in using the scanning tunneling microscope (STM) in the field-emission regime, i.e., at bias voltages larger than the tip work function. In this regime, the applied electric field lifts up the potential barrier above the vacuum level of the sample, introducing a new class of resonances that are absent at low bias voltages, the so-called field-emission resonances (FERs).^{19,20} In previous studies, FERs have been used to explore local changes of the surface work function^{21,22} and scattering properties of surfaces and interfaces^{23,24} and to achieve atomic-scale imaging of diamond.²⁵ A promising application of FERs is to provide information about the dynamics of electrons in image states at surfaces.¹⁵ This is intriguing since FERs are a characteristic of the tip-induced potential barrier itself and, therefore,

they would exist even in the absence of an image potential. Hence, a model is needed which describes the dependence of field emitted electron dynamics along the surface on the topology of the surface potential and accounts for STS spectra in a wide sample bias range.

In this paper, we demonstrate that electrons trapped in long-lived FERs are sensitive to the potential gradient induced by the STM tip along the surface. Scattering of quasifree FER electrons with surface defects gives rise to isotropic two-dimensional (2D) wave patterns, whose wave-vector components in reciprocal space reflect the local perturbation of the surface image potential induced by the STM tip. A combined theoretical and experimental analysis of the FER peaks in dI/dV spectra reveals that their line shape carries information about the scattering properties of the surface, and hence, about their band structure. Our calculations permit the identification of the different intrinsic and extrinsic broadening mechanisms of peaks associated with FERs in conductance spectra in a wide energy range. The organization of the paper is as follows. Section II describes the way the experiments were done. In Sec. III, we present the results and discussion of them in two subsections: Sec. III A is devoted to the analysis of wave patterns that appear in dI/dV maps, while Sec. III B presents a line-shape analysis of dI/dV spectra. Finally, in Sec. IV the conclusions of our work are presented.

II. EXPERIMENT

The experiments were performed in a custom made ultra-high-vacuum scanning tunneling microscope in thermal equilibrium with a liquid-helium bath.²⁶ All spectroscopy data presented in this work were acquired at 4 K. The Cu(100) sample surfaces were cleaned by repetitive cycles of Ar⁺ sputtering (1 keV) and annealing at 900 K. The differential conductance (dI/dV) was measured using a lock-in

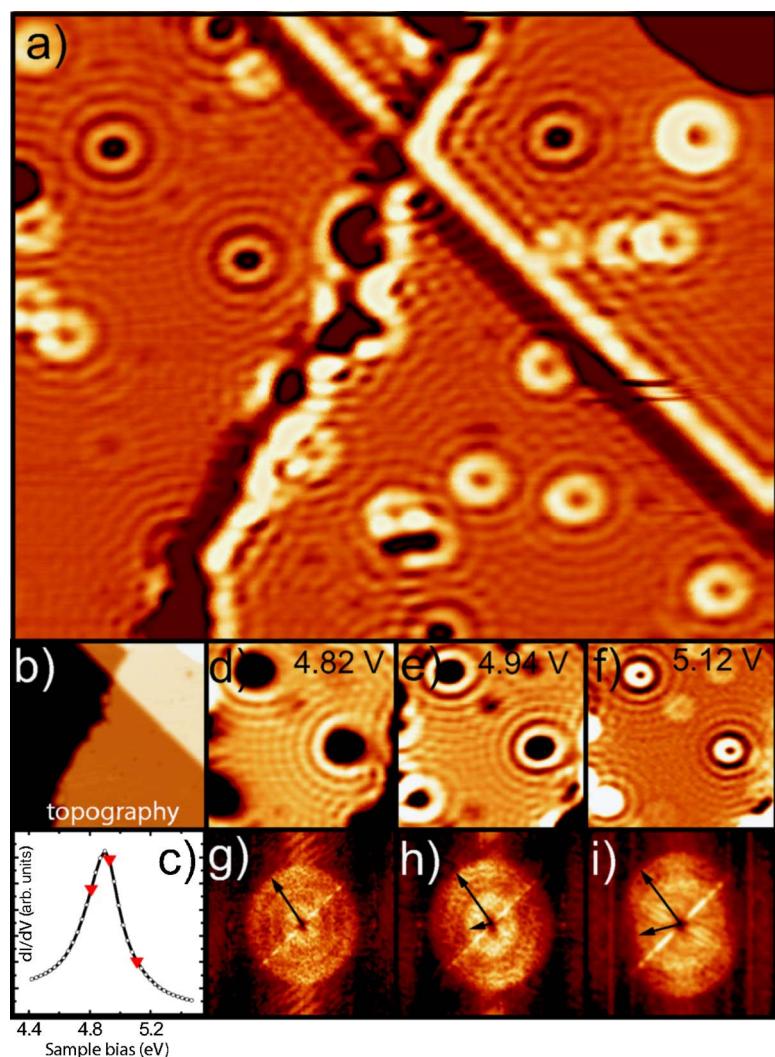


FIG. 1. (Color online) (a) dI/dV map of the Cu(100) surface shown in (b) ($I=10$ nA; $V_S=4.9$ V). Standing waves are clearly seen around steps and surface and subsurface defects. (c) Constant-current dI/dV spectra around the first field-emission resonance. [(d)–(f)] dI/dV maps of a smaller region taken at the bias values indicated in the figure. [(g)–(i)] 2D Fourier transform of (d)–(f). The arrows indicate the inner and outside radii of the disk appearing in K space (see the text).

amplifier above the low-pass frequency of the feedback loop ($f_{ac} \sim 3$ kHz). The dI/dV spectra shown here are taken in constant-current mode (feedback loop closed).^{19,20}

III. RESULTS AND DISCUSSION

A. Wave patterns

The electron dynamics of FER states is essentially quasi-free in the plane parallel to the sample surface, since the corresponding wave functions lie mainly on the vacuum side of the surface. Therefore, these electron states, similar to image states, are not affected by the corrugation of the surface. As for the case of low-lying surface states, hot electrons in field-emission resonances are expected to have a lifetime long enough to be scattered by steps and defects at the surface, giving rise to characteristic standing-wave patterns. In Fig. 1(a), a constant-current dI/dV map shows clear 2D wave patterns around steps and point defects on the Cu(100) surface [Fig. 1(b)]. The image is measured with an applied bias voltage (V_S of 4.9 V, corresponding to the position of the first FER peak [Fig. 1(c)]. A monotonic change to shorter wavelengths with the applied bias [Figs. 1(d)–1(f)] reflects the energy dispersion of these states. At first glance, the

dI/dV maps seem similar to those taken on the (111) faces of noble metals at lower bias. However, an important difference becomes apparent when looking at their 2D Fourier transformation (FT) [Figs. 1(g)–1(i)]: here, the electron wave vector is not constrained to one single $k(E)$ value but shows a broad distribution, causing that the 2D FT maps resemble a disk instead of a ring.¹⁰

We exclude that a surface-projected bulk band, instead of a two-dimensional state, is responsible of this broad distribution of k values in the 2D FT maps. Projected bulk bands' interference patterns might appear only at close distances to the sample and with oscillations corresponding only to wave vectors at the band edge.¹² Instead, the broad distribution of parallel momentum has its origin in the spatial variation of the electric field along the surface due to the finite curvature of the tip. The local shift of the surface potential induced by the STM tip vanishes gradually with the distance away from the tip position [Fig. 2(a)]. Accordingly, for a given electron energy E , the kinetic component along the surface directions ($E_k = E - E_{FER}$, where E_{FER} is the FER binding energy) increases continuously as the electron is accelerated away from the tip. Interference patterns carry information of such inhomogeneous potential by showing oscillations with shorter wavelength as the tip moves away from the scattering poten-

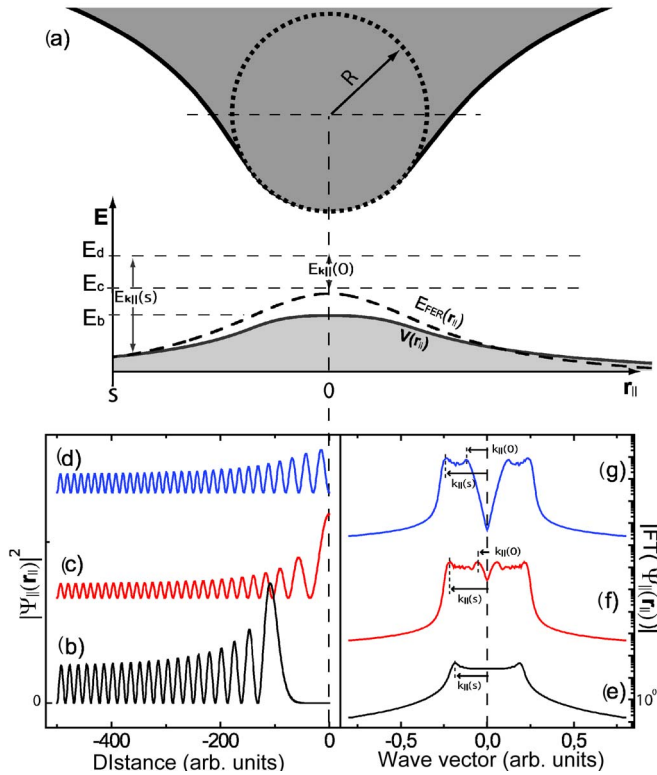


FIG. 2. (Color online) (a) Schematic representation of the non-conservation of parallel momentum due to the applied field by a tip of finite radius R . At a given value of electron energy $E = eV_s - \phi$, the kinetic energy for parallel motion $E_{k_{\parallel}}$ increases from the tip position $r_{\parallel} = 0$ to distant sites at the surface $r_{\parallel} = s$. (b), (c) (d) show the charge density of electron states confined in a large box with a potential $V(x) = V_0/[1 + (x/x_0)^2]$ with energy below, slightly above and above, V_0 , respectively [$V_0 = 0.03$ (arbitrary units) and $x_0 = 200$ (arbitrary units)]. (e), (f), and (g) show the corresponding FT. Curves (c), (d), (f), and (g) are shifted vertically for clarity. The arrows indicate the range of wave vectors with significant weight in the FT and, thus, confirm the measured behavior in Figs. 1(g)–1(i).

tial, and a FT map with nonconstant wave-vector distribution. Deviations from a perfect spherical shape of the tip apex structure are probably responsible for the elliptical shape of the contours.

The evolution of dI/dV maps of Figs. 1(d)–1(f) and their FT images show some interesting behavior. First, Fig. 1(d) shows clear dI/dV oscillations with relatively short wavelength although the image is taken with $eV_s < E_{FER}$, i.e., below the FER onset [as shall be shown later in Sec. III B, the peak position in constant-current dI/dV spectra like in Fig. 1(c) fits closely with the energy E_{FER}]. Second, for eV_s values above E_{FER} the FT maps show an internal circle with a radius k_{min} increasing with the energy [Figs. 1(h) and 1(i)]. The origin of these phenomena can be understood by plotting the electron states of a one-dimensional quantum box with a decaying potential as in Fig. 2(a). In Fig. 2(b), we consider the case of an electronic state with energy lower than E_{FER} . In this case, no allowed state exists locally under the STM tip. Only at distances beyond the point where the energy $E = E_{FER}$ traveling states can exist. In the STM data [Fig. 1(d)], this translates into large dark circles at scattering points, and

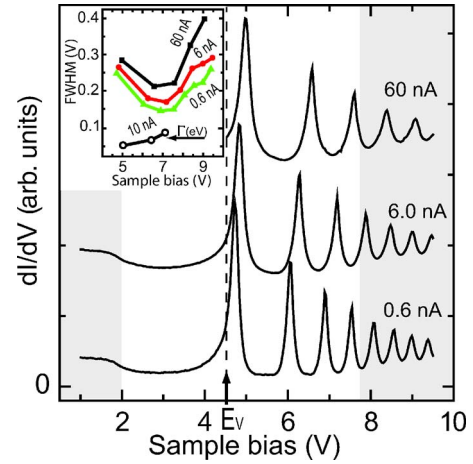


FIG. 3. (Color online) dI/dV spectra taken for several current set points ranging from 0.6 to 60 nA ($V_{ac} = 10$ mV rms). The inset shows the width of the peaks from a Lorentzian fit, as well as values obtained from a phase coherence length analysis (Ref. 28). Shaded areas correspond to the energy location in $\bar{\Gamma}$ of copper bulk bands projected on the (100) surface (Ref. 29).

the onset of standing-wave patterns beyond a certain distance from the defects. In reciprocal space [Fig. 2(e)], a continuous window of wave-vector values from $k_{\parallel}(0) = 0$ to $k_{\parallel}(s)$ reflects the continuous acceleration of the electron waves from the tip position $r_{\parallel} = 0$ to the scattering point $r_{\parallel} = s$ at the surface. Following the same one-dimensional (1D) model, we expect that for electron energy above the resonance onset E_{FER} [Figs. 2(c) and 2(d)], a minimum wave vector $k_{\parallel}(0) = 2m_e^* / \hbar^2 (E - E_{FER})^{1/2}$ appears in the 1D plots [Figs. 2(f) and 2(g)], corresponding to the internal circle in Figs. 1(h) and 1(i).

Therefore, the width of the wave-vector distribution will reflect the spatial change of the local (tip-induced) potential shift. Ideally, for a given value of the tip radius, the critical angle determined by the exponential decay of the Fowler-Nordheim transmittivity²⁷ permits the estimation of the maximum parallel component of the electric field at the tip and, therefore, the change of parallel momentum, based on simple classical trajectory considerations. Assuming a radius of curvature of the tip $R = 10$ nm and a tip-sample distance $Z = 15$ Å, we estimate a change in parallel momentum of 2 nm^{-1} at 5 V, in agreement with our previous analysis shown in Figs. 1(g)–1(i). Results similar to those shown in Fig. 1 are observed for other FERs that appear below 8 eV. However, no wave patterns are seen above this value, indicating a significant decrease of the electron lifetime.

B. Line shape of dI/dV spectra

To understand the role of the surface electronic structure in the dynamics of FERs, next we explore the information contained in dI/dV spectra about the energy width of FERs by analyzing their line shape and comparing with lifetime estimations based on a phase coherence length analysis of interference wave patterns.²⁸

In Fig. 3, we show a series of constant-current dI/dV

spectra at different set point current values. Sharp peaks appear in a wide sample bias range covering the energy range of the projected Cu bulk gap and above.²⁹ Each peak corresponds to the onset of a 2D resonance state. In field-emission regime, the tunnel transmittivity $T(E, V)$ is sharply peaked at the tip Fermi level ($E=E_F$); most of the current comes from a narrow energy window of about 100 meV below E_F ,²⁷ causing FERs to appear as peaks in dI/dV spectra. On the contrary, in the case of surface states close to E_F , dI/dV spectra show a line shape close to a step.¹⁴ Interestingly, we find that the apparent width of the dI/dV peaks exhibits a nonmonotonic behavior (shown in the inset). Resonances lying inside the gap are narrower than those appearing above approximately 8 eV, whose width increases in agreement with the steep decrease of surface reflectivity as the top edge of the projected bulk band gap is crossed.^{6,29}

The finite linewidth of resonance states in the gap is expected to be dominated by intrinsic factors such as the electron reflectivity of the surface, spatial extension of the wave function,³¹ and electric-field strength at the tip-sample region.³⁰ However, as it is shown in the inset of Fig. 3, the apparent width of the first three peaks in constant-current dI/dV spectra is considerably larger than the intrinsic linewidth estimates based on a phase coherence length analysis,²⁸ which for the first FER agree with previous *ab initio* calculations³⁰ and estimations¹⁵ for the same system. Therefore, an additional broadening mechanism must exist to explain the apparent width values in these dI/dV plots, which, presumably, is related with the method of measurement.

During the acquisition of *dynamic* (constant-current) dI/dV spectra, the distance (Z) vs bias voltage (V) characteristics [$Z(V)$] exhibit a pronounced steplike behavior as the resonance is crossed for electron energies lying in the projected gap. The resonant electron transmittivity in this close feedback loop spectroscopy is expected to be affected by the continuous change of the tunneling barrier shape with bias voltage and tip-sample distance. It is reasonable to assume that this dynamic mode will introduce some distortion in the resonance's line shape with respect to the ideal *static* situation, in which the tunneling barrier shape is kept fixed at $Z(V)$ peak values. It is only in this latter case that one could relate the width of peaks in the transmittivity $T(E)$ to the intrinsic width of resonances. We have performed a model calculation to establish a link between intrinsic energy linewidth of resonances in the static tunneling transmittivity $T(E)$ and the corresponding apparent width in constant-current dI/dV spectra, which is related to the auxiliary dynamic transmittivity $T(E_F, V)$ at the tip of the Fermi level.

Our calculations are based on 1D model potentials for the tip and the sample including the work function and the Fermi energy that defines the bottom of the surface potential. For the surface, a periodic sinusoidal modulation that determines the magnitude and position of the energy gap at the $\bar{\Gamma}$ point of the surface Brillouin zone³² is included. Parallel wave-vector components are considered in the full three-dimensional calculations assuming a free-electron-like (parabolic) dispersion. To model electron transmission inside the gap, inelastic scattering at the surface is included by using a

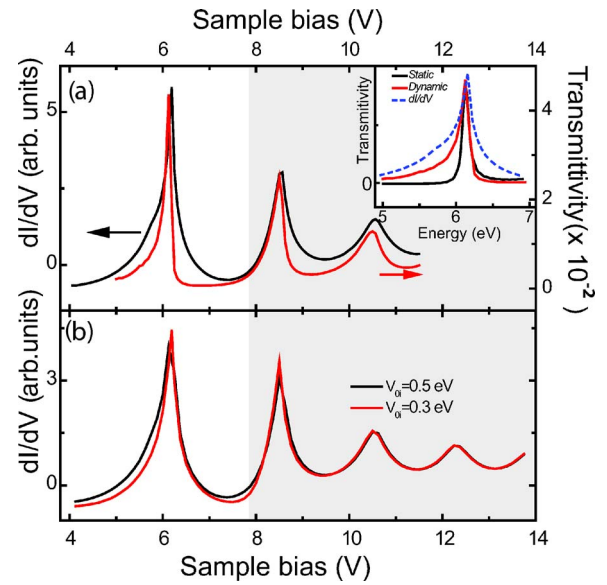


FIG. 4. (Color online) (a) Comparison between a calculated dI/dV spectrum (black curve) and the transmission coefficient (red curve) at the tip Fermi level $T(E_F; V)$. The inset shows a comparison between a static calculation (black) of $T(E)$ at $Z(V)$ values of the first resonance (thus reflecting the intrinsic FER line shape), $T(E_F; V)$ (red), and $dI/dV(V)$ (blue). (b) dI/dV spectra for two V_{0i} values (see the text).

complex potential, similar to previous low-energy electron-diffraction studies.^{33,34} Its imaginary part (V_{0i}) introduces a decay of the electron flux due to absorption. A smooth matching between the tip and sample potentials, which includes multiple images, is used.³⁵ The calculation of the tunneling current for a given tip-sample distance (Z) and bias voltage requires the knowledge of the energy dependence of the barrier transmission coefficient $T(E, V)$ below the tip's Fermi level E_F .³⁶ A quantitative agreement between the measured and calculated dI/dV spectra is not persecuted in this model approach, mostly due to the lack of knowledge of effective tunneling areas, tip-sample distance, or tip work function. Instead, we can provide a qualitative picture of the effect of the dynamic measurements on the peaks' width. The constant-current dI/dV spectra are calculated by numerical differentiation of the current $I(V, Z)$ along the constant-current $Z(V)$ characteristic.

In Fig. 4(a), we show a comparison between calculated $dI/dV(V)$ spectra and the corresponding dynamic transmittivity $T(E_F; V)$. Both curves exhibit a similar shape and a characteristic increase of their linewidth with applied bias. This confirms the high collimation of field emitted electrons in a narrow energy window below E_F . The inset compares the conductance $dI/dV(V)$ around the first peak, the dynamic transmittivity $T(E_F, V)$, and the intrinsic line shape of the corresponding FER obtained in a static calculation at $Z(V)$ peak values. Lorentzian fits to $T(E_F, V)$ and $dI/dV(V)$ give width values of ~ 150 and ~ 350 meV, respectively, while the intrinsic width of the resonance in $T(E)$ is ~ 100 meV. Therefore, the broader line shape in dI/dV spectra must be related both to the above-mentioned finite-energy collimation and the variation of the tunneling barrier shape with applied

bias. For FERs in the gap, the increase in electric-field strength with bias shifts the resonances to higher energy, appearing as broader peaks in $dI/dV(V)$. The increase of tip-sample distance in the dynamic method of measurement partially compensates for this broadening effect. The best conditions for a quantitative line-shape analysis can be achieved at constant field strength conditions ($\sim V/Z$) and low set point current values (low applied field).

By comparing [Fig. 4(b)] the shape of dI/dV curves calculated for two different values of V_{0i} , we find that only the first peak in the gap broadens as a response to the increase in absorption (inelastic scattering). This confirms that inelastic scattering is the broadening mechanism of FERs lying inside the projected band gap. At energies above the gap, inelastic scattering effects play a minor role³⁷ and the FER intrinsic linewidth is dominated by elastic coupling to the bulk continuum (shaded area). In this region, the intrinsic resonances' linewidth is considerably larger (hence, no wave patterns in dI/dV maps could be seen for this energy) and, also, V/Z is almost constant. It is then expected that the effect of the dynamic broadening will be smaller, and the experimental dI/dV peaks' apparent linewidth will be close to the intrinsic value.

IV. CONCLUSIONS

We find that the scattering of electrons in field-emission states with defects in a Cu(100) surface gives rise to isotropic

standing-wave patterns, which reflect their dynamics in response to the electric-field gradients induced by the STM tip at the tip-sample interface. Through a combined theoretical and experimental study we have identified (i) the origin of characteristic peaks width in constant-current dI/dV spectra above the vacuum level as a combination of both their FER intrinsic line shape and the extrinsic distortion due to the measuring process, and (ii) for FERs in the gap this distortion introduces an additional broadening, leading to a non-monotonic behavior of the width with sample bias. Our results show that STS in the field-emission regime can be used to gain information about the electron dynamics and surface electronic properties at energies well above the vacuum level.

ACKNOWLEDGMENTS

We gratefully acknowledge Lucia Aballe, Andrei Borisov, Martin Hansmann, Daniel Sánchez Portal, and Wolf Widdra for very helpful discussions. This work was supported in part by the Basque Departamento de Educacion, Universidades e Investigacion, the University of the Basque Country UPV/EHU, the Spanish Ministerio de Educacion y Ciencia, the EU Network of Excellence NANOQUANTA (Grant No. NMP4-CT-2004-500198), and the EUROCORES project MOL-VIC.

-
- ¹H. Nienhaus, Surf. Sci. Rep. **45**, 1 (2002).
²P. M. Echenique, R. Berndt, E. V. Chulkov, Th. Fauster, A. Goldmann, and U. Höfer, Surf. Sci. Rep. **52**, 219 (2004).
³U. Bovensiepen, Prog. Surf. Sci. **78**, 87 (2005).
⁴F. J. Himpsel and J. E. Ortega, Phys. Rev. B **46**, 9719 (1992).
⁵K. Boger, M. Weinelt, and Th. Fauster, Phys. Rev. Lett. **92**, 126803 (2004).
⁶S. Andersson and B. Kasemo, Solid State Commun. **8**, 961 (1970).
⁷M. F. Crommie, C. P. Lutz, and D. M. Eigler, Nature (London) **363**, 524 (1993).
⁸Y. Hasegawa and Ph. Avouris, Phys. Rev. Lett. **71**, 1071 (1993).
⁹Ph. Hofmann, B. G. Briner, M. Doering, H.-P. Rust, E. W. Plummer, and A. M. Bradshaw, Phys. Rev. Lett. **79**, 265 (1997).
¹⁰L. Petersen, P. T. Sprunger, Ph. Hofmann, E. Lægsgaard, B. G. Briner, M. Doering, H.-P. Rust, A. M. Bradshaw, F. Besenbacher, and E. W. Plumer, Phys. Rev. B **57**, R6858 (1998).
¹¹J. I. Pascual, Z. Song, J. J. Jackiw, K. Horn, and H.-P. Rust, Phys. Rev. B **63**, 241103(R) (2001).
¹²J. I. Pascual, A. Dick, M. Hansmann, H.-P. Rust, J. Neugebauer, and K. Horn, Phys. Rev. Lett. **96**, 046801 (2006).
¹³L. Bürgi, O. Jeandupeux, H. Brune, and K. Kern, Phys. Rev. Lett. **82**, 4516 (1999).
¹⁴J. Kliewer, R. Berndt, E. V. Chulkov, V. M. Silkin, P. M. Echenique, and S. Crampin, Science **288**, 1399 (2000).
¹⁵P. Wahl, M. A. Schneider, L. Diekhöner, R. Vogelgesang, and K. Kern, Phys. Rev. Lett. **91**, 106802 (2003).
¹⁶J. I. Pascual, G. Bihlmayer, Yu. M. Koroteev, H.-P. Rust, G. Ceiballos, M. Hansmann, K. Horn, E. V. Chulkov, S. Blügel, P. M. Echenique, and Ph. Hofmann, Phys. Rev. Lett. **93**, 196802 (2004).
¹⁷C. Corriol, V. M. Silkin, D. Sánchez-Portal, A. Arnau, E. V. Chulkov, P. M. Echenique, T. von Hofe, J. Kliewer, J. Kröger, and R. Berndt, Phys. Rev. Lett. **95**, 176802 (2005).
¹⁸L. Limot, T. Maroutian, P. Johansson, and R. Berndt, Phys. Rev. Lett. **91**, 196801 (2003).
¹⁹G. Binnig, K. H. Frank, H. Fuchs, N. Garcia, B. Reihl, H. Rohrer, F. Salvan, and A. R. Williams, Phys. Rev. Lett. **55**, 991 (1985).
²⁰R. S. Becker, J. A. Golovchenko, and B. S. Swartzentruber, Phys. Rev. Lett. **55**, 987 (1985).
²¹T. Jung, Y. W. Mo, and F. J. Himpsel, Phys. Rev. Lett. **74**, 1641 (1995).
²²M. Pivetta, François Patthey, Massimiliano Stengel, Alfonso Baldereschi, and Wolf-Dieter Schneider, Phys. Rev. B **72**, 115404 (2005).
²³J. A. Kubby, Y. R. Wang, and W. J. Greene, Phys. Rev. Lett. **65**, 2165 (1990).
²⁴A. J. Caamaño, Y. Pogorelov, O. Custance, J. Mendez, A. M. Baró, J. Y. Veillen, J. M. Gómez-Rodríguez, and J. J. Sáenz, Surf. Sci. **426**, L420 (1999).
²⁵K. Bobrov, A. J. Mayne, and G. Dujardin, Nature (London) **413**, 616 (2001).
²⁶H.-P. Rust, J. Buisset, E. K. Schweizer, and L. Cramer, Rev. Sci. Instrum. **68**, 129 (1997).
²⁷J. W. Gadzuk, Phys. Rev. B **47**, 12832 (1993).

- ²⁸We can estimate a phase coherence length following the analysis in Refs. 13 and 15 neglecting the effect of the electric field on the wave patterns profile along the surface. It is implicitly assumed that when extracting the intrinsic lifetime $\tau=1/\Gamma$ from the measured phase coherence length $L_\phi=v_\phi\tau$, a mean value of k_\parallel exists such that $mv_\phi=hk_\parallel$, where m is the free-electron mass. The mean value of k_\parallel is extracted from the wavelength of the real-space wave patterns and L_ϕ from the exponential decay of the amplitude of the oscillations that appear close to a straight step shown in Fig. 1. Although this mean value of k_\parallel is not well defined, it would correspond to a value between the minimum and maximum values shown as arrows in Fig. 2(g). This “rough” estimation is heuristically justified since the result obtained is similar to the one obtained in Ref. 15 and since the wave-vector dependence of the electron lifetime is not too pronounced (Ref. 30).
- ²⁹A. Goldmann, V. Dose, and G. Borstel, Phys. Rev. B **32**, 1971 (1985).
- ³⁰S. Crampin, Phys. Rev. Lett. **95**, 046801 (2005).
- ³¹P. M. Echenique and J. B. Pendry, Prog. Surf. Sci. **32**, 111 (1989).
- ³²E. V. Chulkov, V. M. Silkin, and P. M. Echenique, Surf. Sci. **437**, 330 (1999).
- ³³J. B. Pendry, *Low Energy Electron Diffraction* (Academic, London, 1974).
- ³⁴R. García, J. J. Sáenz, J. M. Soler, and N. García, Surf. Sci. **181**, 69 (1986).
- ³⁵J. M. Pitarke, F. Flores, and P. M. Echenique, Surf. Sci. **234**, 1 (1990).
- ³⁶C. B. Duke, in *Tunneling in Solids*, edited by F. Seitz, D. Turnbull, and H. Ehrenreich (Academic, New York, 1969).
- ³⁷A. G. Borisov, E. V. Chulkov, and P. M. Echenique, Phys. Rev. B **73**, 073402 (2006).